EurJIC European Journal of Inorganic Chemistry

ChemPubSoc Europe

FULL PAPER

DOI:10.1002/ejic.201200921

Synthesis of Chalcogenidoimidodiphosphinato–Rh^{I} Complexes and DFT Investigation of Their Catalytic Activation in Olefin Hydroformylation

Alexios Grigoropoulos,*[a] Dimitrios Maganas,*[a,b] Dimitrios Symeonidis,[a] Petros Giastas,[c] Andrew R. Cowley,[d] Panayotis Kyritsis,*[a] and Georgios Pneumatikakis[a]

Keywords: Rhodium / Hydroformylation / Density functional calculations / Hemilabile ligands

The synthesis and spectroscopic characterization of [Rh{$R_2P(S)NP(S)R_2$-*S*,*S*′}(cod)] [cod = 1,5-cyclooctadiene; R = Ph (**1**), *i*Pr (**4**)], [Rh{$Ph_2P(S)NP(S)Ph_2$-*S*,*S*′}$(CO)_2$] (**2**) and [Rh{$Ph_2P(S)NP(S)Ph_2$-*S*,*S*′}(CO)(PPh_3)] (**3**) is described. The crystal structures of complexes **1** and **3** are also presented. The synthesized Rh^{I} complexes are essentially not catalytically active against olefin hydroformylation, in contrast to the previously reported complex [Rh{$Ph_2P(O)NPPh_2$-*P*,*O*}(CO)-(PPh_3)] (**6**). Differences in the catalytic activity were interpreted with the aid of a well-defined DFT-based protocol involving relativistic effects and dispersion correction. The steric and electronic effects of the Rh^{I} coordination environment with respect to their activation by H_2 are discussed. The results demonstrate that the presence of the more electronegative oxygen atom in the Rh^{I} coordination sphere polarizes the H–H bond and promotes its heterolytic cleavage, thereby leading to the formation of a Rh^{I}–monohydride complex in which the oxygen atom of the ligand is protonated.

Introduction

Mono- and dichalcogenidoimidodiphosphinato ligands, that is, $[R_2P(E)NPR_2]^-$ and $[R_2P(E)NP(E')R_2]^-$ (E, E′ = O, S, Se; R = aryl or alkyl group), denoted in the following as $(^{R}L–P,E)^-$ and $(^{R}L–E,E')^-$, respectively, are considered as inorganic (carbon-free) analogues of acetylacetonate (acac). They exhibit rich coordination chemistry towards main group and transition metals that has been extensively reviewed by Ly and Woollins;[1,2] Silvestru and Drake;[3] and Haiduc.[4,5] These ligands provide a π-delocalized chelating system that can be easily modified by varying the chalcogenide donor atoms E and the peripheral R groups. Moreover, their structural flexibility allows for bite angles that vary between <90° and >109.5° leading to metal–chalcogenidoimidodiphosphinato complexes of different geometries (T_d, D_{4h} or O_h), as well as different ring conformations (boat, chair or twisted boat) of the respective metallocycles. For instance, [Ni(^{Ph}L–*S*,*S*′)$_2$] remains the only [Ni$^{II}S_4$]-containing complex that has been isolated in either a tetrahedral[6,7] or a square-planar[8] geometry in which the $(^{Ph}L–S,S')^-$ ligand adopts the twisted boat (in T_d) or the boat (in D_{4h}) conformation, respectively. Likewise, [Ni($^{i\text{Pr}}$L-*Se*,*Se*′)$_2$] also shows two stereoisomers (T_d and D_{4h}); however, the $(^{i\text{Pr}}L–Se,Se')^-$ ligand adopts the twisted-boat conformation in both geometries.[9] In addition, tetrahedral [Ni(^{Ph}L-*O*,*E*)$_2$] (E = S, Se) complexes revert to octahedral ones upon dissolution in coordinating solvents like dmf and thf that occupy the axial positions.[10,11] These results demonstrate that the overall geometry is directly correlated with the metallocycle conformation and that their relationship is governed by the nature of the chalcogenide donor atom E, the peripheral groups R and the metal centre.[1,3,12]

In the course of the last ten years, there has been a renewed interest in the exploration of the physicochemical properties and potential applications of metal complexes bearing this type of ligands. Consequently, significant work has been published that is related to various research fields of inorganic chemistry, as we will briefly outline. The electronic structure of the tetrahedral [M(^{Ph}L–*S*,*S*′)$_2$] (M = Fe,[13] Co,[12,14–16] Ni[17]) and octahedral [Ni(^{Ph}L–*O*,*E*)$_2$-$(sol)_2$][11] (E = S, Se; sol = dmf, thf) complexes has been

[a] Inorganic Chemistry Laboratory, Department of Chemistry, National and Kapodistrian University of Athens, Panepistimiopolis 15771, Athens, Greece
Fax: +30-210-7274782
E-mail: agrigorop@chem.uoa.gr
kyritsis@chem.uoa.gr
Homepage: http://www.chem.uoa.gr/
[b] Max-Planck Institute for Chemical Energy Conversion, 45470 Mülheim an der Ruhr, Germany
E-mail: dimitrios.manganas@cec.mpg.de
[c] Laboratory of Structural and Supramolecular Chemistry, NCSR "Demokritos", Agia Paraskevi 15310, Athens, Greece
[d] Chemistry Research Laboratory, Department of Chemistry, University of Oxford, Mansfield Road, Oxford OX1 3TA, United Kingdom

Supporting information for this article is available on the WWW under http://dx.doi.org/10.1002/ejic.201200921.

determined by the combination of various spectroscopic, magnetometric and computational methods. These studies have defined magnetostructural correlations for the above paramagnetic complexes and provided additional insight into the $M^{II}S_4$-containing active sites of metalloproteins such as native, $Fe^{II}S_4$-containing rubredoxin[18] and its Co^{II}- or Ni^{II}-substituted analogues.[19]

Another major recent advancement has been the synthesis of the Te-containing ligands by Chivers and co-workers,[20] which has led to a large number of novel metal complexes.[21] Many of these compounds have been employed by O'Brien et al. as single-source precursors for the deposition of metal telluride thin films on glass substrates by chemical vapour deposition.[22,23] This technique has also been applied for the preparation of metal sulfide and selenide materials using instead complexes containing the S- and Se-containing ligands.[24–28] The $(^{Ph}L–S,S')\cdot I_2$ adduct has been suggested as a potential metal-extraction agent.[29–31] Diamagnetic tetrahedral metal complexes, namely, $[M(^{iPr}L–Se,Se')_2]$ (M = Zn, Cd, Hg), as well as square-planar ones, $[M(^{iPr}L–Se,Se')_2]$ (M = Pd, Pt) have been studied by solid-state NMR spectroscopy,[32,33] whereas complexes of d- and f-block elements bearing $(^{Ph}L–O,O')^-$ have been used as luminescent materials.[34–38] In addition, lanthanide and actinide metal complexes of the $[M(^{iPr}L–E,E')_3]$ type (E, E′ = S, Se, Te) have been studied experimentally[39,40] and theoretically[41,42] in an effort to probe the covalency of the bonds between f-block elements and chalcogen atoms. Last, in the field of homogeneous catalysis, Leung and co-workers have employed $(^{Ph}L–S,S')^-$ to modify Ru^{II}-containing polymerization catalysts,[43] $(^{Ph}L–O,O')^-$ to synthesize transition-metal catalysts for organic oxidations[44,45] and $(^{iPr}L–O,O')^-$ to prepare novel M^{IV}-oxo/peroxo complexes (M = Ti, Zr, Ce).[46]

The recent advances in catalytic applications by rhodium complexes bearing phosphane–chalcogenide donor ligands,[47] as well as the well-documented catalytic properties in olefin hydroformylation of $[Rh(acac)(CO)(PR_3)]$[48] and $[Rh(Bp)(CO)(PR_3)]$[49] [Bp = bis(pyrazolylborate)], encouraged us to investigate the catalytic properties of the isoelectronic Rh^I complexes containing the $(^RL–P,E)^-$ and $(^RL–E,E')^-$ ligands. Herein we describe the synthesis and spectroscopic characterization of the Rh^I complexes bearing disulfidoimidodiphosphinato ligands, namely, $[Rh(^{Ph}L–S,S')(cod)]$ (cod = 1,5-cyclooctadiene) (**1**), $[Rh(^{Ph}L–S,S')(CO)_2]$ (**2**), $[Rh(^{Ph}L–S,S')(CO)(PPh_3)]$ (**3**) and $[Rh(^{iPr}L–S,S')(cod)]$ (**4**). It should be remembered that $[Rh(^{Ph}L–Se,Se')(CO)(PPh_3)]$ (**5**) is catalytically inactive and $[Rh(^{Ph}L–P,O)(CO)(PPh_3)]$ (**6**) is catalytically active against styrene hydroformylation.[50] The catalytic activity of **6** has been attributed to the hemilabile behaviour of $(^{Ph}L\text{-}P,O)^-$ that forms a strained planar five-membered ring containing a weak Rh^I(soft)–O(hard) bond.[51,52] Such an effectively weak Rh–O bond can be cleaved and reformed, allowing for the generation of a vacant site in the Rh^I coordination sphere under hydroformylation conditions.[53,54] On the contrary, $(^{Ph}L–Se,Se')^-$ forms a more stable six-membered ring containing two relatively stronger Rh^I(soft)–Se(soft) bonds. Therefore, the generation of a vacant coordination site is less probable, thereby explaining why **5** is catalytically inactive.[50]

The catalytic activity of complexes **1**–**4** was tested in styrene hydroformylation. However, complexes **1**, **2** and **4** are inactive and complex **3** shows only negligible catalytic activity. Also taking into account our findings for **5** and **6**, apparently the activation of the chalcogenidoimidodiphosphinato–Rh^I complexes is hindered as the chalcogenide donor atom becomes softer and less electronegative. Therefore, the catalytic activation of the $[Rh(^{Ph}L)(CO)(PPh_3)]$ complexes **3**, **5** and **6** was investigated with the aid of dispersion-corrected density functional theory (DFT-D_3), also considering relativistic effects, to probe the effect of different chalcogen donor atoms. DFT methodologies have been widely used to explain the energetic barriers along the Rh^I-catalyzed hydroformylation mechanism.[55–58] In addition, when compared with higher correlated methods, DFT shows at least comparable qualitative and often quantitative results.[59,60] The computational and experimental results described in this work explain the observed trends in catalytic activity against olefin hydroformylation by probing the effects of specific structural changes in the Rh^I coordination environment. Along these lines, the hemilabile behaviour of the mono- and dichalcogenidoimidodiphosphinates is investigated, which reveals their potential application for the modification of transition-metal catalyst precursors.

Results and Discussion

Synthesis

The synthetic procedure that affords the yellow-orange Rh^I complexes **1**–**4** is depicted in Scheme 1. These complexes are air-stable for at least one week. Typical cleavage of the chlorido bridges of the dinuclear complex $[\{Rh(\mu\text{-}Cl)(cod)\}_2]$ upon workup with $(^{Ph}L–S,S')K$ or $(^{iPr}L–S,S')K$ yields **1** and **4**, respectively. Treatment of a solution of **1** in

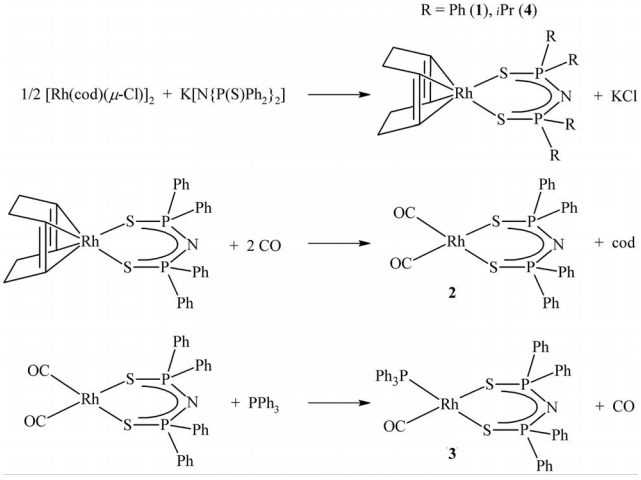

Scheme 1. Synthetic pathway for the preparation of complexes **1**–**4**.

CH_2Cl_2 with a stream of CO affords the dicarbonyl complex **2**. Replacement of one CO ligand upon treatment of **2** by an equivalent amount of PPh_3 leads to [Rh(^{Ph}L–*S*,*S*′)(CO)(PPh_3)] (**3**). It should be noted that raising the metal/phosphane ratio even to 3:1 does not lead to the substitution of the second CO group. This is a well-documented trend since only stronger π acceptors such as $P(OPh)_3$ and $P(NC_4H_4)_3$ are capable of replacing both carbonyl ligands.[61,62] Complex **4** does not participate in any ligand-exchange reactions, which indicates that the presence of the electron-donating and bulky *i*Pr peripheral groups increases the Rh–(cod) bond strength and sterically hinders ligand-substitution reactions.

Solid-State Crystal Structures

The crystal structures of **1** and **3** reveal a square-planar geometry around the Rh^I centre. Complex **1** crystallizes in space group $P\bar{1}$ as yellow plates. The structure is shown in Figure 1 and selected bond lengths and angles are listed in Table 1. Average P–N and P–S bond lengths for the free protonated ligand (^{Ph}L–*S*,*S*′)H are 1.676 and 1.916 Å, respectively.[63] Deprotonation and coordination of the latter to Rh^I result in the shortening of the P–N (av. 1.594 Å) and the lengthening of the P–S bonds (av. 2.021 Å), due to delocalization of the π-electron density among the S–P–N–P–S fragment, as it has already been postulated by structural data[64] and theoretical calculations.[12] The P2 atom lies almost in the mean S–Rh–S plane, with the corresponding dihedral angle S1–Rh–S2–P2 equal to 6.5°. On the contrary, the P1 and N1 atoms are placed well above the horizontal plane. The S2–Rh–S1–P1 dihedral angle is 51.4°, while the nitrogen atom is located 1.317 Å above the mean S–Rh–S plane. Therefore, the RhS_2P_2N metallocycle is not planar and adopts a slightly distorted boat conformation, with the S1 and P2 atoms occupying the apices. It should be noted that compounds containing σ^4,λ^5-phosphorus atoms can be nonplanar and still exhibit delocalization of the π-electron density.[65–67] The magnitude of the average Rh–S bond lengths (2.389 Å) and the S1–Rh–S2 angle (98.3°) is typical of similar complexes in which (^{R}L–*S*,*S*′)$^-$ ligands form six-membered rings and adopt the boat conformation.[6,68] The cod ligand is side-on coordinated to the metal centre. The C25–C26 double bond is 0.025 Å shorter than the C29–C30 bond, whereas the opposite pattern is found for the average length of the respective Rh–C bonds. This is indicative of stronger back-donation towards the C29–C30 double bond. Therefore, the degree of back-donation of electron density towards the π* orbitals of the olefin is correlated with the orientation of the *trans* P–S bond measured by the corresponding S–Rh–S–P dihedral angle. Back-donation is increased when the *trans* P–S bond moves towards the S–Rh–S horizontal plane and the S–Rh–S–P dihedral angle becomes smaller. In this way, the transfer of π-electron density from the S 3p orbitals that are perpendicular to the molecular plane towards the π* orbitals of the olefin is enhanced. This observation implies that the conformation of the (^{Ph}L–*S*,*S*′)$^-$ ligand is correlated with the back-donation of electron density towards the C=C double bonds of cod, or in fact any other type of ligand that is a π acid. Clearly, this trend is expected to become more apparent when the ligands coordinated *trans* to (^{Ph}L–*S*,*S*′)$^-$ have different π-accepting properties (see below).

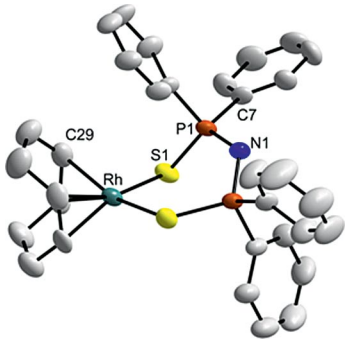

Figure 1. Crystal structure of **1** with ellipsoids drawn at the 30% probability level. Hydrogen atoms have been omitted for clarity.

Table 1. Selected bond lengths [Å] and angles [°] for complexes **1** and **3**.

Complex **1**		Complex **3**	
Rh–S1	2.386(2)	Rh–S1	2.4006(1)
Rh–S2	2.391(3)	Rh–S2	2.418(1)
S1–P1	2.017(3)	S1–P1	2.032(1)
S2–P2	2.026(3)	S2–P2	2.016(1)
P1–N	1.599(7)	P1–N	1.591(3)
P2–N	1.589(5)	P2–N	1.598(3)
Rh–C25	2.162(10)	Rh–CO	1.812(4)
Rh–C26	2.155(10)	C–O	1.156(5)
Rh–C29	2.131(9)	Rh–PPh_3	2.277(1)
Rh–C30	2.147(10)	S1–Rh–S2	98.80(3)
C25–C26	1.381(10)	P1–N–P2	123.1(2)
C29–C30	1.406(10)	Rh–S1–P1	109.24(5)
S1–Rh–S2	98.29(8)	Rh–S2–P2	102.05(5)
P1–N–P2	124.6(4)	C–Rh–PPh_3	88.7(1)
Rh–S1–P1	100.1(1)	S1–Rh–PPh_3	91.38(3)
Rh–S2–P2	110.6(1)	S2–Rh–CO	81.2(1)
S1–Rh–S2–P2	6.5(1)	S1–Rh–S2–P2	–44.93(5)
S2–Rh–S1–P1	–51.4(1)	S2–Rh–S1–P1	–2.03(5)

In contrast to the crystal structure of **1** presented in this work, the structure of the same complex that has been reported by Cheung et al., containing a CH_2Cl_2 solvent molecule in the unit cell (**1**·CH_2Cl_2), exhibits a different ring conformation.[69] More specifically, in **1**·CH_2Cl_2 the P atoms are located on opposite sides of the S–Rh–S horizontal plane. Therefore, the conformation of the metallocycle can be best described as a distorted twisted boat.[2,17,70] The two S–Rh–S–P dihedral angles are 11.2 and 35.5° and in this case back-donation towards the cod ligand is more evenly distributed.

Complex **3** crystallizes in space group $P\bar{1}$ as yellow plates. The crystal structure of this compound is presented

herein for the first time (Figure 2). Selected bond lengths and angles are listed in Table 1. The coordination geometry around the central Rh atom is approximately square planar [root mean square (rms) deviation from the mean plane is 0.04 Å]. The P1 atom, located *trans* to the CO ligand, is displaced by only 0.07 Å from the mean S–Rh–S plane, with the corresponding dihedral angle S2–Rh–S1–P1 equal to 2.0°. On the contrary, to absorb the ring strain, the S2–P2 bond located *trans* to PPh_3 is rotated out of the S–Rh–S horizontal plane. The S1–Rh–S2–P2 dihedral angle is 44.9°; hence the RhS_2P_2N metallocycle adopts the boat conformation. The S1–Rh–S2 angle (98.8°) and the average Rh–S bond length (2.409 Å) are again consistent with the boat conformation of the six-membered ring.[6,68] It is well established that the values of the M–S bond lengths and the S–M–S bond angles that are associated with the boat conformation are larger than those found in the chair conformation of the disulfidoimidodiphosphinato–metal complexes, in which the S1–M–S2 angle is approximately 90° and the average M–S bond lengths are approximately 0.3 Å shorter.[2,17,71] The P–N bonds are significantly shortened (av. 1.595 Å) whereas the P–S bonds are lengthened (av. 2.024 Å) compared with the free $(^{Ph}L–S,S')^-$ ligand, which again displays the delocalization of π-electron density among the S–P–N–P–S fragment. It has been pointed out that the difference between the two Rh–O bond lengths in [Rh(acac)(CO)(PR_3)] complexes (R = alkyl group or aryl group) arises from the different *trans* influence exerted by PR_3 and CO.[72] For example, the Rh–O bond lengths in [Rh(acac)(CO)(PPh_3)] differ by 0.06 Å.[73] Such is the case for complex **3**, in which the Rh–S bond length *trans* to PPh_3 is 0.017 Å longer than the one *trans* to CO. In the analogous diselenido complex **5**, the Rh–Se bond-length difference is 0.010 Å.[50] The smaller differentiation between the Rh–S/Se bond lengths of the aforementioned complexes, compared with [Rh(acac)(CO)(PPh_3)], reflects the structural flexibility and the extensive delocalization of π-electron density among the metal complexes bearing chalcogenidoimidodiphosphinato ligands.

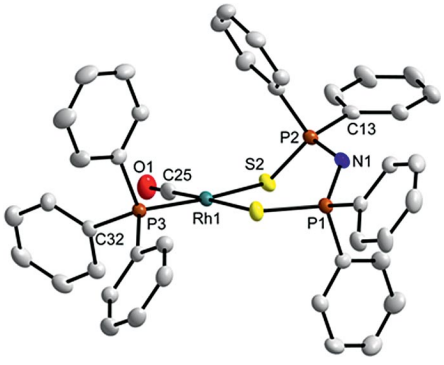

Figure 2. Crystal structure of **3** with ellipsoids drawn at the 30% probability level. Hydrogen atoms have been omitted for clarity.

IR Spectroscopy

The IR spectra of **1**–**4** exhibit the well-documented trend regarding the P–N and P–S bond strength.[64,70] The comparison between the ν(PNP) or ν(PS) bands of the complexes and the free protonated ligands (Table 2) confirms that the P–N bonds are strengthened, whereas the P–S bonds are weakened. This is typical for this family of ligands, since π delocalization of the extra N lone pair that is generated upon deprotonation results in both an increased P–N and a decreased P–S bond order.[12] The IR spectrum of **2** reveals two very strong bands at 2066 and 1997 cm^{-1} of approximately equal intensity, due to the symmetric and asymmetric stretch of the two mutually *cis* CO ligands. The IR spectrum of **3** shows a single ν(CO) band at 1976 cm^{-1}. Compared with the dicarbonyl complex **2**, the ν(CO) band in **3** is down-shifted, consistent with the increased back-donation to the remaining sole CO ligand that is a stronger π acid than PPh_3. On the contrary, compared with the diselenido complex **5**, the ν(CO) band in **3** is up-shifted, which indicates the weaker donor ability of $(^{Ph}L–S,S')^-$ compared with $(^{Ph}L–Se,Se')^-$.

^{31}P NMR Spectroscopy

^{31}P chemical shifts of complexes **1**–**4** are listed in Table 2. In complexes **1**, **2** and **4**, the P atoms of the metallocycle are chemically equivalent, therefore, only one doublet is observed due to weak coupling with ^{103}Rh (not resolved in the case of complex **4**). On the contrary, the ^{31}P NMR spectrum of complex **3** is much more complicated and it can only be resolved at lower temperatures. The chemical equivalency of the P atoms of the ligand $(^{Ph}L–S,S')^-$ is removed since different ligands are coordinated *trans* to each S atom and, therefore, **3** can be best described as an ABMX spin system (Figure 3).

Table 2. Characteristic IR [cm^{-1}] and $^{31}P\{^1H\}$ NMR spectroscopic data [ppm] in $CDCl_3$ for ligands and complexes **1**–**4**. NMR spectra were obtained at 298 K with the exception of of **3** (218 K).

Complex	ν(PNP)	ν(PS)	ν(CO)	P_A [$^2J_{Rh,P}$, Hz]	P_B [$^2J_{Rh,P}$, Hz]	P_X [$^1J_{Rh,P}$, Hz]
1	1167	575	–	38.8 (d) [3.6]		
2	1169	572	2066	37.7 (d) [3.6]		
3	1151	563	1977	36.1 (dd) [3.3] $^3J(P_AP_X)$ = 24 Hz	38.3 (dd) [4.1] $^3J(P_BP_X)$ = 8 Hz	40.5 (ddd) [157]
4	1194	486	–	62.7 (not resolved)		
5[50]	1168	544	1962			

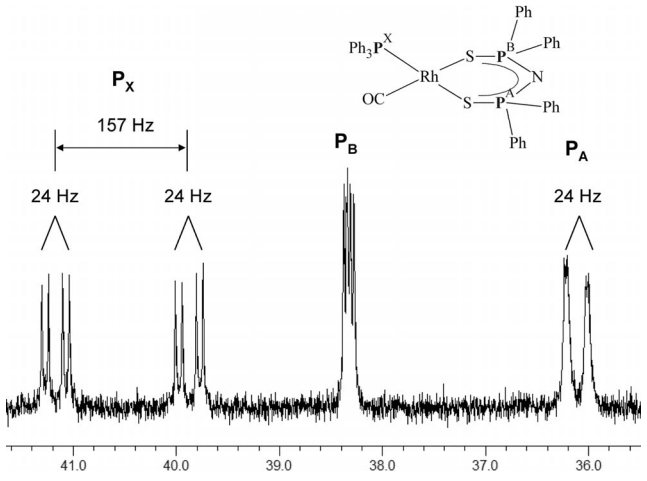

Figure 3. $^{31}P\{^{1}H\}$ NMR spectrum of complex **3** recorded in $CDCl_3$ at 218 K.

The P_X atom of PPh_3 is directly coordinated to the metal centre, thus it is deshielded. The coupling with ^{103}Rh ($^{1}J_{M,X}$ = 157 Hz) is similar to other known complexes bearing PPh_3 bonded to Rh^{I}.[74,75] The coupling with the P_A atom of the $(^{Ph}L–S,S')^-$ ligand, located *trans* to PPh_3, is stronger ($^{3}J_{A,X}$ = 24 Hz) than the coupling with the P_B atom, located *cis* to PPh_3 ($^{3}J_{B,X}$ = 8 Hz), following the usual $J(trans) > J(cis)$ pattern.[76,77] Therefore, overall, P_X gives rise to a low-field ddd peak (δ_P = 40.5 ppm). The two high-field peaks correspond to the two P atoms of the $(^{Ph}L–S,S')^-$ ligand. Since $^{3}J_{A,X}$ (*trans*) > $^{3}J_{B,X}$ (*cis*), the dd peak centred at δ = 36.1 ppm is assigned to P_A (*trans* to PPh_3) and the peak centred at δ = 38.3 ppm is assigned to P_B (*cis* to PPh_3). The comparison between the ^{31}P chemical shifts of complexes **2** and **3** reveals that the P_A atom (*trans* to PPh_3 and hence *cis* to CO) is shielded, whereas the P_B atom (*cis* to PPh_3 and hence *trans* to CO) is deshielded. This is attributed to the stronger π acidity of CO than PPh_3, which demonstrates the transfer of electron density along the P–S–Rh–CO bond pathway. Unfortunately, even at –80 °C, the coupling between the P atoms of $(^{Ph}L–S,S)^-$ could not be resolved. Cheung et al. reported a different peak assignment for **3**, in which the ^{31}P chemical shifts increase in the reverse order, that is, $\delta_X < \delta_B < \delta_A$; however, no detailed hyperfine coupling analysis was presented.[69] Moreover, the ^{31}P NMR spectrum of the analogous diselenido complex **5**,[50] in which the presence of ^{77}Se satellites facilitates peak assignment, strongly supports our analysis.

It has been firmly established that the donor strength of an anionic bidentate ligand in the $[RhL(CO)(PZ_3)]$ type of complexes is strongly correlated with the energy of the respective ν(CO) band and the magnitude of the $^{1}J_{Rh,P}$ coupling constant.[49,78] It is therefore interesting to expand the series reported by Trzeciak et al.,[49] by including the $(^{Ph}L–S,S')^-$ and $(^{Ph}L–Se,Se')^-$ ligands (Table 3). Both dichalcogenidoimidodiphosphinato–Rh^{I} complexes exhibit very low ν(CO) and $^{1}J_{Rh,P}$ values that are indicative of an electron-rich metal centre, as a consequence of the soft nature of the S/Se donor atoms.

Table 3. Comparison of ν(CO) [cm^{-1}] and $^{1}J_{Rh,P}$ [Hz] for complexes of the $[RhL(CO)PPh_3]$ type.

Ligand	$(acac)^-$	$(Bp)^-$	$(^{Ph}L–S,S')^-$	$(^{Ph}L–Se,Se')^-$
ν(CO)	1983	1987	1977	1962
$^{1}J_{Rh,P}$	177.4	156	157	160.2

Geometric Considerations

The crystallographic and spectroscopic data of complexes **1**–**4** indicate that the magnitude of back-donation influences the conformation of the RhS_2P_2N metallocycle. To verify this hypothesis, the optimized geometry structures of complexes **2** and **3** were initially sought and they are shown in Figure 4. Geometry optimizations were performed starting from both the boat and the twisted-boat metallocycle conformation. The most important geometric features of the optimized structures are presented in Table 4. It should be stressed that the initial metallocycle conformation (twisted boat or boat) does not affect the final optimized geometry. In fact, in the case of **2**, the metallocycle adopts an ideal twisted-boat conformation. The P atoms of $(^{Ph}L–S,S')^-$ are directed above and below the S–Rh–S plane, with both S–Rh–S–P dihedral angles equal to 24°, whereas the N atom lies in the horizontal S–Rh–S plane. Both Rh–S (2.434 Å) and Rh–CO bonds (1.825 Å) are mutually equal. Consequently, complex **2** shows an overall C_2 symmetry, with the main axis bisecting the C–Rh–C and S–Rh–S angles. This is a straightforward consequence of the presence of identical ligands *trans* to $(^{Ph}L–S,S')^-$ that impose the same electronic and steric effect and thus do not distort the intrinsic C_2 symmetry of the deprotonated ligand.[64] Given that the twisted-boat conformation leads to larger bite angles,[17] the S–Rh–S angle in **2** (100.9°) opens up considerably.

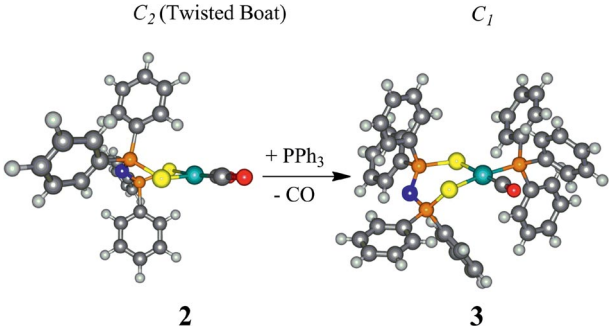

Figure 4. Optimized geometry structures of complexes **2** (C_2 symmetry) and **3** at the RI-BP86/TZVPP/TZVP level (C: grey, H: white, N: blue, O: red, P: orange, Rh: green, S: yellow).

The calculated bond lengths and bond angles in the optimized geometry structure of **3** are in good agreement with the experimental ones (see the Supporting Information, Table S2). The stronger *trans* influence of PPh_3 than CO[72] results in the elongation of the respective *trans* Rh–S bond (2.451 Å), whereas the other one is slightly shortened (2.429 Å) compared with **2** (Table 4). In the case of **3**, the metallocycle adopts a boat conformation, independent from the initial conformation. Therefore, the different con-

Table 4. Selected bond lengths [Å], angles [°] and ν(CO) [cm^{-1}] of the optimized geometry structures of **2** and **3** at the RI-BP86/TZVPP/TZVP level.

	Complex **2**	Complex **3**
Rh–S1 (*trans* CO)	2.434	2.429
Rh–S2 (*trans* P)	2.434	2.451
Rh–CO	1.825	1.794
Rh–PPh_3	–	2.220
C–O	1.158	1.166
S2–Rh–S1–P1	–24	5
S1–Rh–S2–P2	–24	–51
ν(CO)	1979.8	1966.4

formations of **2** and **3** can only be explained by the presence of different ligands *trans* to (^{Ph}L–*S*,*S*′)$^-$. In the case of the dicarbonyl complex **2**, the CO groups impose the same electronic and steric effect and thus do not distort the intrinsic C_2 symmetry of the deprotonated ligand.[64] However, as was previously discussed, replacement of one CO ligand by PPh_3 leads to unequal Rh–S bond lengths and breaks up the inherent C_2 symmetry of the (^{Ph}L–*S*,*S*′)$^-$ ligand. This allows for the RhS_2P_2N metallocycle to adopt the boat conformation that favours square-planar geometries.[17] The C–O bond in **3** is lengthened, the Rh–CO is shortened and the corresponding ν(CO) is decreased, thereby verifying that back-donation of the π-electron density to the sole CO ligand is enhanced when the ligand adopts the boat conformation (Table 4).

Electronic Structure

As previously discussed, complex **2** shows approximate C_{2v} symmetry around the $RhS_2(CO)_2$ core. Replacement of one CO ligand by PPh_3 lowers the symmetry to C_1 and the six-membered RhS_2P_2N metallocycle adopts the boat conformation. The composition of the Rh^I frontier molecular orbitals of **3** is in agreement with what is expected from ligand-field theory for a d^8 Rh^I square-planar complex (Figure 5). The LUMO is the typical σ*-antibonding orbital of d^8 square-planar complexes that is mainly composed of the Rh^I 4d$_{x^2-y^2}$ orbital, the in-plane S 3p orbitals of (^{Ph}L–*S*,*S*′)$^-$ and the C and P lone pairs. The HOMO is mainly composed of the Rh^I 4d$_{z^2}$ orbital (ca. 80%). The HOMO–1, HOMO–2 and HOMO–3 orbitals comprise the Rh^I d$_\pi$ orbitals, the out-of-plane S 3p orbitals of (^{Ph}L–*S*,*S*′)$^-$ and the unoccupied π* orbitals of CO and PPh_3. Most importantly, the boat conformation of the metallocycle maximizes the orbital overlap along the S–Rh–CO bond pathway. The P–S bond that is located *trans* to CO lies in the molecular plane, causing the corresponding S 3p lone pair to be oriented parallel to the Rh^I 4d$_{xz}$ orbital. In this way, the overlap between these two orbitals is maximized. HOMO–2 represents the antibonding interaction, whereas the respective bonding combination lies lower in energy. On the contrary, the P–S bond located *trans* to PPh_3 is rotated out of the molecular plane and the respective overlap between the associated S 3p lone pair and the Rh^I 4d$_{yz}$ orbital is less efficient (HOMO–1). Therefore, the

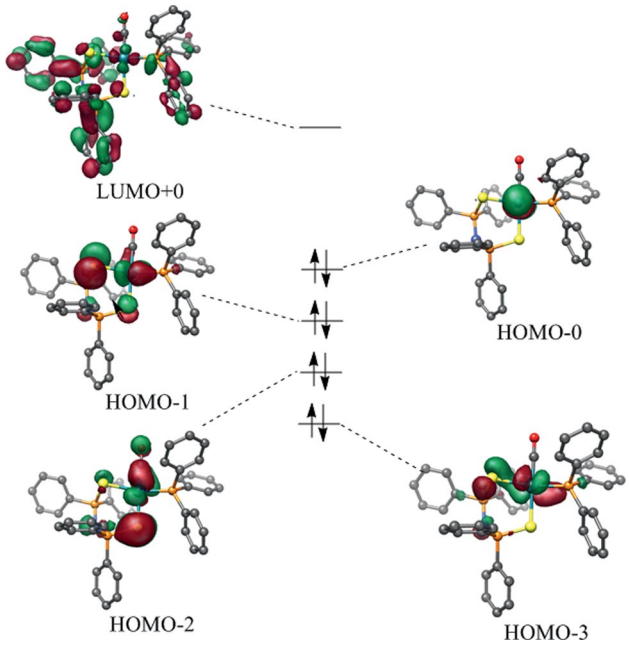

Figure 5. Frontier molecular orbitals of complex **3** at the RI-BP86/TZVPP/TZVP level. Hydrogen atoms have been omitted for clarity.

stronger π acidity of CO than PPh_3 drives the respective *trans* P–S bond in plane, to facilitate the transfer of electron density from the chelating ligand towards the CO π* orbitals along the S–Rh–CO bond pathway.

To summarize, the coordination of different ligands *trans* to (^{Ph}L–*S*,*S*′)$^-$ cancels out the built-in C_2 symmetry of the latter that is associated with the twisted-boat conformation. The greater π acidity of CO than PPh_3 drives the *trans*-to-CO P–S bond in plane, to promote (^{Ph}L–*S*,*S*′)$^-$→Rh^I→CO back-donation of electron density. This gives rise to a boat conformation of the RhS_2P_2N metallocycle in **3**. More importantly, the departure from C_2 symmetry renders the two Rh–S bonds chemically nonequivalent, which suggest a potential hemilabile behaviour of the (^{Ph}L–*S*,*S*′)$^-$ ligand.

Metallocycle Conformation

To further verify the correlation between the magnitude of the S–Rh–S–P dihedral angles and the back-donation towards π-accepting ligands, relaxed potential energy surface (PES) scans along the S–Rh–S–P dihedral angle *trans* to CO (ω_{CO}) were performed in 5° steps for the model complexes [Rh(^{Me}L)(CO)(PMe_3)] (^{Me}3PMe_3), [Rh(^{Me}L)(CO)(PH_3)] (^{Me}3PH_3) and [Rh(^{Me}L)(CO)(PF_3)] (^{Me}3PF_3), in which different phosphanes are coordinated to Rh^I. From the diagram presented in Figure 6, it is evident that the S–Rh–S–P dihedral angle that corresponds to the lowest energy structure for each phosphane follows Tolman's electronic parameter (TEP),[78] that is, PMe_3 < PH_3 < PF_3. The ω_{CO} dihedral angle is minimized (ca. 20°) when a stronger donor, like PMe_3, is introduced in the coordination sphere. On the contrary, when the phosphane is a strong

acceptor, like PF_3, the ω_{CO} is maximized (ca. 35°), whereas the corresponding value for PH_3 (ca. 25°) is calculated in between. The steric effect does not seem to play an important role since the value of ω_{CO} neither follows Tolman's cone angle (θ) nor changes significantly when PCl_3 is introduced. The latter is larger than PF_3 but shows similar electron-withdrawing properties.

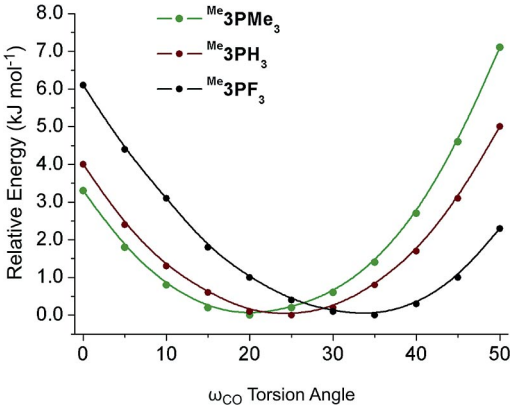

Figure 6. Relaxed PES scan at the RI-BP86/TZVPP/TZVP level along the S–Rh–S–P dihedral angle *trans* to CO (ω_{CO}) in 5° steps for $^{Me}3PMe_3$ (green), $^{Me}3PH_3$ (red) and $^{Me}3PF_3$ (black).

The previous analysis shows that the conformation of the RhS_2P_2N metallocycle is dictated by the electron-donating or -withdrawing properties of the coordinated phosphane ligand. The comparison of the optimized geometry structures of $^{Me}3PMe_3$, $^{Me}3PH_3$, $^{Me}3PF_3$ and $^{Me}2$ (Table 5) confirms that the P–S bond that is located *trans* to the stronger π acid PF_3 moves in plane. On the contrary, the P–S bond that is located *trans* to the stronger electron-donating phosphane PMe_3 is rotated out of plane and back-donation to the CO ligand is enhanced, as can be deduced from the calculated ν(CO) frequencies. The same trend is observed when the respective diselenido model complexes are examined (Table 5). It should be also noted that the calculated ν(CO) frequencies for the diselenido complexes are lower in energy than the ones of the respective disulfido complexes, which verifies that the diselenidoimidodiphosphinato ligand is a stronger donor.

Table 5. S/Se–Rh–S/Se–P dihedral angles ω_{CO} (*trans* to CO) and ω_P (*trans* to PZ_3), ν(CO) frequencies [cm^{-1}] and C–O bond lengths [Å] for the optimized geometry model complexes [Rh{^{Me}L–(*E*,*E*)}](CO)(PZ_3)] (E = S or Se and Z = Me, H, F) and [Rh{^{Me}L–(*E*,*E*)}($CO)_2$] (used as a reference) at the RI-BP86/TZVPP/TZVP level.

Complex	ω_{CO} [°]	ω_P [°]	ν(CO)	C–O	TEP [cm^{-1}]	θ [°]
$^{Me}2$	24	24	2016.9[a]	1.158	–	–
$^{Me}3PMe_3$	20	29	1956.2	1.169	2064	118
$^{Me}3PH_3$	24	25	1972.5	1.166	2083	87
$^{Me}3PF_3$	35	14	2010.5	1.159	2111	104
$^{Me}3PCl_3$	35	14	2005.2	1.159	2097	124
$^{Me}5(CO)_2$	23	23	2008.4[a]	1.159	–	–
$^{Me}5PMe_3$	21	26	1950.0	1.170	2064	118
$^{Me}5PH_3$	26	21	1965.8	1.167	2083	87
$^{Me}5PF_3$	34	13	2003.1	1.160	2111	104
$^{Me}5PCl_3$	33	14	1997.5	1.160	2097	124

[a] Average value of the symmetric and asymmetric stretch mode.

Catalytic Activation Mechanism

The catalytic activity against styrene hydroformylation for complexes **1**–**4** was explored. Complexes **1**, **2** and **4** are essentially inactive, whereas complex **3** shows negligible catalytic activity (yield is less than 20% at 40 °C in CH_2Cl_2). Most likely, (^{Ph}L–*S*,*S*′)$^-$ is strongly coordinated to Rh^I, thus preventing the generation of a vacant site, even in the case of complex **3** in which the two Rh–S bonds are nonequivalent (see above). This also explains the catalytic inactivity of complex **5**,[50] since (^{Ph}L–*Se*,*Se*′)$^-$ is an even better donor, as was previously discussed. On the contrary, complex **6** shows substantial catalytic performance,[50] which indicates that the (^{Ph}L–*P*,*O*)$^-$ ligand is less tightly bound to Rh^I owing to the presence of a relatively weaker Rh(soft)–O(hard) bond. It is well established that under olefin-hydroformylation conditions the catalytically active species is a [Rh^I–H] complex.[79] Therefore, DFT calculations were performed to elucidate how these complexes are activated by H_2 and why only **6** forms a catalytically active [Rh^I–H] species. Also taking into account that the initial interaction of H_2 with any metal centre results in the formation of a [M–(η^2-H_2)] complex that may correspond to a true reactive intermediate or a transition structure,[80–84] we initially explored the stability of such [Rh^I–(η^2-H_2)] complexes in which one Rh–E (E = O, S, Se) bond is cleaved and H_2 is side-on coordinated.

Our computational study was based on the corresponding truncated models $^{Me}3PMe_3$, $^{Me}5PMe_3$ and $^{Me}6PMe_3$, in which all phenyl groups were replaced by methyl groups. This type of truncation is not expected to significantly affect qualitatively the following analysis of the catalytic activation of complexes **3**, **5** and **6**, since the steric effect of a larger phosphane will have the same influence on all complexes. Nevertheless, we have also calculated the buried volume ($\%V_{Bur}$)[85] of different phosphane ligands in **3** as a quantitative measurement of the steric demand of such a truncation. As shown in Table S13 in the Supporting Information, $\%V_{Bur}$ of PZ_3 ligands at the optimized Rh–P distances is lowered from 30.8 (Z = Ph) to approximately 24 (Z = Me, Cl). Hence, the order of magnitude of the steric demand is retained when PPh_3 is substituted by smaller phosphanes. Furthermore, the truncated models were fully optimized along the corresponding interconversion pathways by employing the same DFT methods as described above. In this way, one hopes to incorporate the steric and electronic effects of the bulkier groups into the DFT calculations without facing the prohibitive costs of the calculations on the full systems.

For the disulfido complex $^{Me}3PMe_3$, the only [Rh^I–(η^2-H_2)] complex that is identified as a stable intermediate is [(k^1-^{Me}L–*S*,*S*′)Rh(η^2-H_2)(CO)(PMe_3)] ($^{Me}3PMe_3$–H_2), in which the Rh–S bond that is located *trans* to PMe_3 is

cleaved and the vacant site is now occupied by H_2 (Figure 7, $A_{S,S}$). In all other cases, including the one in which H_2 approaches perpendicularly to the molecular plane, H_2 does not bind to the metal centre but instead dissociates and the original complex is reformed. $^{Me}3PMe_3$–H_2 displays square-planar geometry and H_2 is side-on coordinated. The corresponding diselenido complex [(k^1-^{Me}L–*Se*,*Se*′)Rh(η^2-H_2)(CO)(PMe_3)] ($^{Me}5PMe_3$–H_2) is also identified as the only stable [Rh^I–(η^2-H_2)] product of the interaction of H_2 with $^{Me}5PMe_3$ (Figure 7, $A_{Se,Se}$). However, the presence of an oxygen atom in the Rh^I coordination sphere of $^{Me}6PMe_3$ renders the inherently weaker Rh–O bond as the most plausible candidate for bond cleavage. Moreover, the intermediate in which H_2 is side-on coordinated to the metal centre is not stable. Instead, H_2 is directly heterolytically split leading to the square-planar complex [(k^1-^{Me}L–*P*,*OH*)-Rh(H)(CO)(PMe_3)] ($^{Me}6PMe3$-OH,H) in which the oxygen atom of the ligand is protonated (Figure 7, B). The hydride is coordinated *trans* to CO and the protonated oxygen atom is occupying the axial position at a nonbonding distance

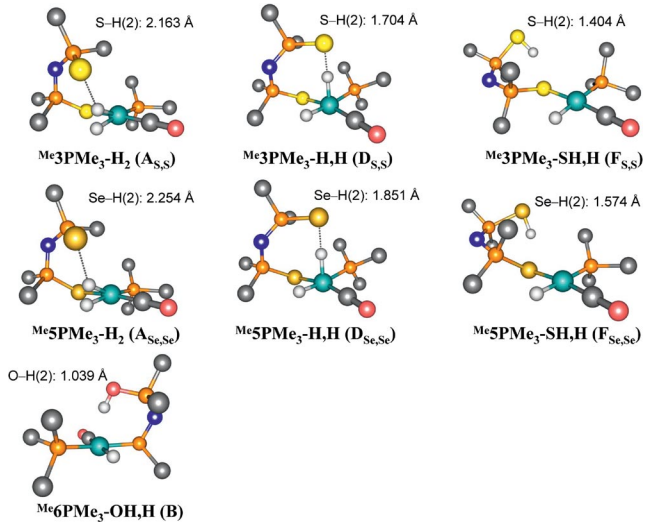

Figure 7. Optimized geometry structures at the dispersion-corrected RI-BP86-D/TZVPP/TZVP level for the intermediates identified along the H–H bond cleavage relaxed PES scan. (C: grey, H: white, N: blue, O: red, P: orange, Rh: green, S: yellow, Se: orange-yellow). Hydrogen atoms of the methyl groups have been omitted for clarity.

(Table 6). More importantly, this [Rh^I–H] complex could serve as the actual catalytic species during olefin hydroformylation.

In this context, the formation of this [Rh^I–H] key species was investigated further in silico for complexes **3**, **5** and **6**. Figure 8 shows the relaxed PES scan along the H–H bond length, starting from the aforementioned [Rh^I–(η^2-H_2)] intermediates. The total electronic energy values are calculated relative to the total electronic energy of the free reactants, that is, the initial rhodium complex and H_2. The optimized geometry structures of all the local minima are shown in Figure 7, the most important bond lengths are listed in Table 6 and *xyz* coordinates are provided in the Supporting Information (Tables S3–S12). For the disulfido complex $^{Me}3PMe_3$, the first local minimum (point A) corresponds to $^{Me}3PMe_3$–H_2 that is found 65.1 kJ mol^{-1} higher in energy than the free reactants ($^{Me}3PMe_3$ + H_2). The H–H bond is considerably elongated owing to back-donation of the electron-rich Rh^I centre (H–H = 0.904 Å vs. 0.734 Å for H_2 itself). The P1–S1 bond bearing the sulfur atom that is bound to the metal centre is weakened, whereas the P2–S2 bond bearing the noncoordinated sulfur atom is strengthened. The opposite trend is observed for the respective P–N bonds. Overall, the ligand shows a more localized distribution of electron density (Rh–S–P=N–P=S resonance structure). Increasing the H–H distance to 2.1 Å leads to [(k^1-^{Me}L–*S*,*S*)Rh(H)$_2$(CO)(PMe_3)] ($^{Me}3PMe3$-H,H). This [Rh^{III}–$(H)_2$] complex (point D; 50.9 kJ mol^{-1}) is formally the product of H_2 oxidative addition to Rh^I and is calculated 14.2 kJ mol^{-1} lower in energy than $^{Me}3PMe_3$–H_2, whereas the related transition state (point C; 73.6 kJ mol^{-1}) is calculated at only 8.5 kJ mol^{-1}. An independent geometry optimization for this complex shows no imaginary frequencies. $^{Me}3PMe3$-H,H shows square-pyramidal geometry with one coordinated hydride occupying the axial position (Figure 7, $D_{S,S}$). The ligand reverts back to the completely delocalized resonance structure, in which both P–S and P–N bonds are almost equal in length (Table 6). This shows that the axial hydride electronically communicates with the free end of the (^{Me}L–*S*,*S*′)$^-$ ligand that lies in close proximity (S–H_{ax} = 1.704 Å). Further increasing the H–H distance leads to the reductive elimination of the axial hydride and the concomitant protonation of the free end of the (^{Me}L–*S*,*S*)$^-$ ligand, which results

Table 6. Most important bond lengths [Å] for the optimized geometry intermediates at the dispersion-corrected RI-BP86-D/TZVPP/TZVP level for the optimized geometry intermediates identified along the proposed mechanism for the activation of **3**, **5** and **6** by H_2.

Complex	H1–H2	Rh–H1	Rh–H2$_{ax}$	P1–E1$_{cord}$	P2–E2	P1–N	P2–N
$^{Me}3PMe_3$	–	–	–	2.079	2.073	1.640	1.649
$^{Me}3PMe_3$–H_2	0.904	1.705	1.801	2.105	2.029	1.623	1.659
$^{Me}3PMe_3$-H,H	2.185	1.603	1.668	2.080	2.077	1.637	1.634
$^{Me}3PMe_3$-SH,H	–	1.624	–	2.078	2.143	1.667	1.614
$^{Me}5PMe_3$	–	–	–	2.228	2.224	1.641	1.649
$^{Me}5PMe_3$–H_2	0.914	1.699	1.787	2.254	2.178	1.626	1.659
$^{Me}5PMe_3$-H,H	2.177	1.601	1.642	2.229	2.222	1.636	1.635
$^{Me}5PMe_3$-SeH,H	–	1.627	–	2.238	2.276	1.661	1.623
$^{Me}6PMe_3$	–	–	–		1.596	1.677	1.629
$^{Me}6PMe_3$-OH,H	–	1.664	2.073	–	1.646	1.694	1.608

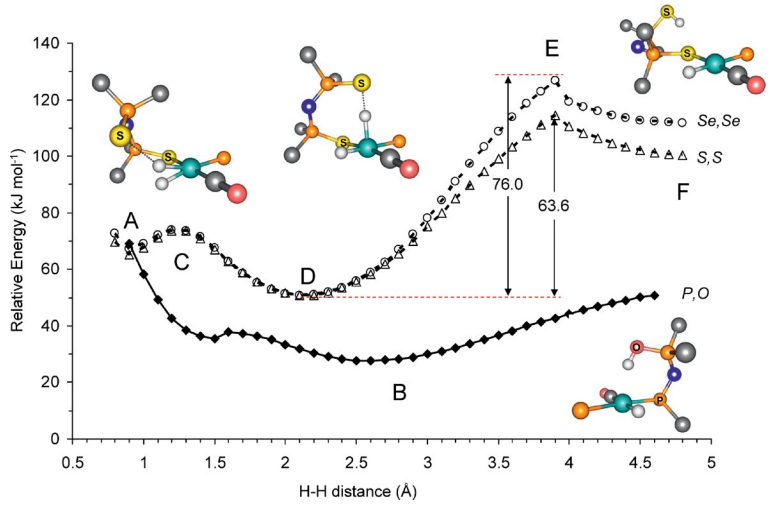

Figure 8. Relaxed PES scan along the H–H bond-cleavage pathway in 0.1 Å steps at the RI-BP86-D/TZVP level for $^{Me}3PMe_3$ (open triangles), $^{Me}5PMe_3$ (open cycles) and $^{Me}6PMe_3$ (closed squares). Structures of the local minima for $^{Me}3PMe_3$ and $^{Me}6PMe_3$ are shown. Total energy values are calculated relative to the sum of the total energy of the respective [^{Me}LRhCOPMe$_3$] complex and H_2.

in [(k^1-^{Me}L-*S*,*SH*)Rh(H)(CO)(PMe$_3$)] ($^{Me}3PMe_3$-SH,H). The π-electron density is again completely localized (Rh–S=P–N=P–SH resonance structure), since the pendant sulfur atom is now protonated. However, the PES scan shows that this [Rh^I–H] complex (point F; 100.4 kJ mol^{-1}) lies 44.5 kJ mol^{-1} higher in energy than $^{Me}3PMe_3$-H,H, whereas the associated transition state (point E; 114.5 kJ mol^{-1}) is calculated at 63.6 kJ mol^{-1}. Therefore, it is the reductive elimination step of the axial hydride that is both kinetically and thermodynamically not favoured, clarifying the poor catalytic activity of complex **3** against olefin hydroformylation.

The same pathway is found for the diselenido model $^{Me}5PMe_3$. The H_2 oxidative-addition product $^{Me}5PMe3$-H,H (point D; 50.7 kJ mol^{-1}) is calculated 16.6 kJ mol^{-1} lower in energy than $^{Me}5PMe_3$–H_2 (point A; 67.3 kJ mol^{-1}), whereas the associated transition state is again insignificant, calculated at 6.7 kJ mol^{-1} (point C; 74.0 kJ mol^{-1}). However, the calculated transition state (point E; 126.7 kJ mol^{-1}) for the hydride reductive-elimination step is found at 76.0 kJ mol^{-1} and the final [Rh^I–H] complex $^{Me}5PMe3$-SeH,H (point F; 111.9 kJ mol^{-1}) is calculated 61.2 kJ mol^{-1} higher in energy than $^{Me}5PMe3$-H,H. Figure 8 also includes the relaxed PES scan for the model complex $^{Me}6PMe_3$, con-

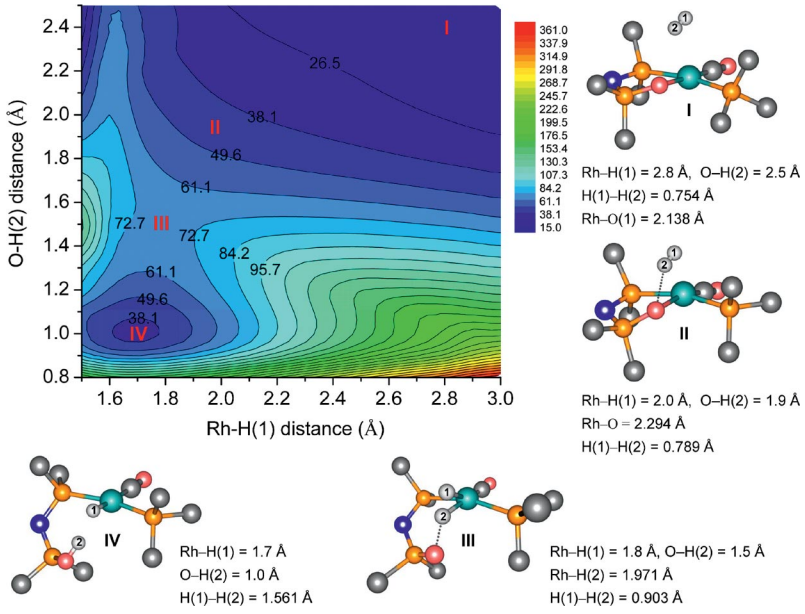

Figure 9. Contour plot of the relaxed PES scan along the Rh–H1 and O–H2 distances in 0.1 Å steps at the dispersion-corrected RI-BP86-D/TZVPP/TZVP level for the activation of $^{Me}6PMe_3$ by H_2. Total energy values are calculated relative to the sum of the total energy of $^{Me}6PMe_3$ and H_2.

taining the (^{Me}L-*P*,*O*)$^-$ ligand. The shallow minimum at H–H = 1.5 Å corresponds to a minor conformational change of the metallocycle. As previously discussed, the [Rh^I–(η^2-H$_2$)] complex does not correspond to a local minimum (point A) but instead H$_2$ is directly heterolytically split, giving rise to ^{Me}6PMe$_3$-OH,H (point B) that lies 27.6 kJ mol^{-1} higher in energy than the free reactants (^{Me}6PMe$_3$ + H$_2$).

The fact that ^{Me}6PMe$_3$ does not form a stable [Rh^I–(η^2-H$_2$)] complex prompted us to further explore its interaction with H$_2$. Figure 9 depicts the contour plot of the PES scan along the H$_2$ heterolytic cleavage pathway in which the Rh–H1 and O–H2 distances have been simultaneously scanned. The sum of the total electronic energies of ^{Me}6PMe$_3$ and H$_2$ was chosen as our zero-point of reference. H$_2$ approaches the Rh^I centre by the sterically preferred trajectory, that is, perpendicularly to the molecular plane. For Rh–H1 and O–H2 distances that are both greater than 2.2 Å, H$_2$ is only weakly interacting with ^{Me}6PMe$_3$, as it can be deduced from the length of the H–H bond (H–H = 0.754 Å). This gives rise to a plateau in the PES (Figure 9, I) that lies approximately 15 kJ mol^{-1} higher in energy than the free reactants. When the Rh–H1 distance decreases below 2.2 Å, the Rh–O bond is lengthened and the H–H bond is slightly elongated (Figure 9, II). The contour plot shows a saddle point at 61.1 kJ mol^{-1} for which the Rh–H1 and the O–H2 bond lengths vary between 1.7–1.9 Å and 1.4–1.6 Å, respectively (Figure 9, III). This area corresponds to the [Rh^I–(η^2-H$_2$)] complex [(k^1-^{Me}L–*P*,*O*)Rh(η^2-H$_2$)(CO)(PMe$_3$)] in which the H–H bond is considerably elongated (H–H = 0.903 Å) and the Rh–O bond is broken. The fact that this [Rh^I–(η^2-H$_2$)] complex lies on a saddle point verifies our previous results regarding the instability of such a species in the case of ^{Me}6PMe$_3$. It should be also remembered that the respective [Rh^I–(η^2-H$_2$)] complexes containing sulfur (^{Me}3PMe$_3$–H$_2$) or selenium (^{Me}5PMe$_3$–H$_2$) as donor atoms were identified as stable intermediates (Figure 7, A). On the contrary, [(k^1-^{Me}L–*P*,*O*)Rh(η^2-H$_2$)(CO)(PMe$_3$)] is related to a transition state that connects the aforementioned plateau and the local minimum at 38.1 kJ mol^{-1}, located at the bottom left corner of the contour plot (Figure 9, IV). This corresponds to a [Rh^I–H] complex in which the H–H bond has been heterolytically cleaved and the ligand is protonated. The protonated oxygen atom lies in close proximity with the hydride. However, this Rh–H···H–O interaction is weak and an inward rotation of the free end of the ligand would lead to the more stable ^{Me}6PMe3-OH,H complex in which the protonated oxygen atom occupies the axial position (Figure 7, B).

In summary, in the case of ^{Me}6PMe$_3$, the Rh–O bond is cleaved as H$_2$ approaches the metal centre. The PES contour plot also reveals that the respective [Rh^I–(η^2-H$_2$)] species is not a stable intermediate, but H$_2$ is instead directly heterolytically split. Therefore, the catalytic activation of the Rh^I complexes **3**, **5** and **6** by H$_2$ follows different pathways. For complexes **3** and **5**, bearing the softer chalcogenides (S, Se) as donor atoms, the formation of a catalytically active [Rh^I–H] species proceeds through (i) H$_2$ side-on coordination, (ii) H$_2$ oxidative addition and (iii) hydride reductive elimination (Scheme 2, top). The delocalization of π-electron density allows for the P–S/Se and P–N bonds to alter between formally single and double to accommodate the induced structural changes. However, complex **6**, containing the harder oxygen atom, is activated through the direct heterolytic splitting of H$_2$ (Scheme 2, bottom). Both mechanisms have been proposed for the activation of Rh^I catalyst precursors.[86,87] However, in the case of complexes **3** and **5**, the H$_2$ oxidative addition [Rh^{III}–(H)$_2$] product, which is clearly catalytically inactive, is calculated as the most stable intermediate. Furthermore, the ensuing reductive elimination of one coordinated hydride that would give rise to a catalytically active [Rh^I–H] species is not thermodynamically and kinetically probable.

The fact that **3** shows very limited catalytic activity, whereas **5** is completely inactive, can be attributed to the lower electronegativity of selenium than sulfur that is obviously crucial for the ligand-assisted hydride reductive elimination to take place.[86] This is also supported by the fact that the Δ*H* and Δ*G* values (Table 7) of the oxidative addition step are almost identical for **3** and **5**, since the ligand is not actively involved in this step, whereas non-negligible differences are found in the subsequent reductive elimination step. On the contrary, the presence of the more elec-

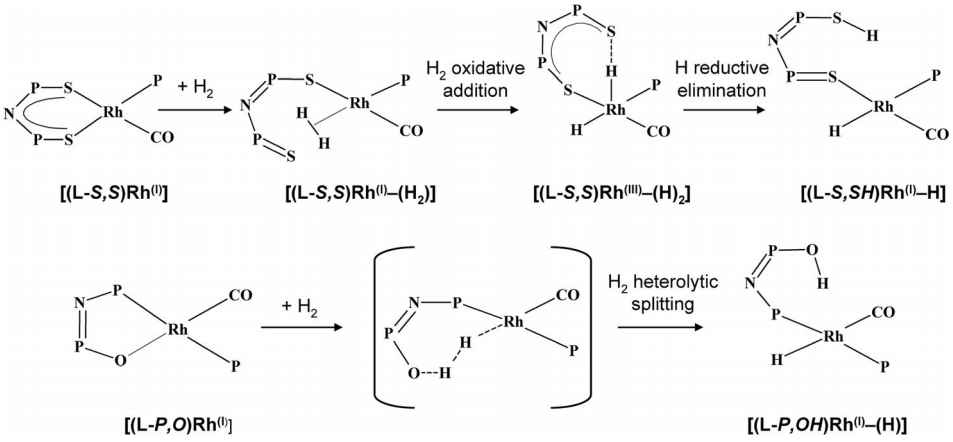

Scheme 2. Proposed mechanism for the activation of complexes **3**, **5** and **6** by H$_2$ towards a catalytically active [Rh^I–H] species.

tronegative oxygen atom in the Rh^I coordination sphere in complex **6** promotes the direct H_2 heterolytic splitting, thereby giving rise to a stable and catalytically active [Rh^I–H] complex (^{Me}6PMe$_3$–OH,H). Moreover, the ΔH and ΔG values (Table 7) of the respective formation reaction, although positive, are not prohibitive, especially under hydroformylation conditions.

Table 7. Thermodynamic values [kJ mol^{-1}] for the activation of ^{Me}3PMe$_3$, ^{Me}5PMe$_3$ and ^{Me}6PMe$_3$ according to the reaction [Rh^{Me}LCOPMe$_3$] + H_2 → product at the dispersion-corrected RI-BP86-D/TZVPP/TZVP level.

Product	ΔH	ΔG
^{Me}3PMe$_3$–H_2	39.4	71.5
^{Me}5PMe$_3$–H_2	38.7	70.0
^{Me}3PMe$_3$–H,H	20.4	51.7
^{Me}5PMe$_3$–H,H	21.5	55.0
^{Me}3PMe$_3$–SH,H	84.5	122.9
^{Me}5Me$_3$–SeH,H	91.5	127.0
^{Me}6PMe$_3$–OH,H	20.8	49.6

Conclusion

In this study, we report on the synthesis and spectroscopic characterization of the Rh^I complexes **1**–**4** containing the disulfidoimidodiphosphinato ligands [$R_2P(S)NP(S)R_2$]$^-$ (R = Ph, *i*Pr). The crystal structures of complexes **1** and **3** show a square-planar geometry around the Rh^I central atom in which the RhS_2P_2N metallocycle adopts the boat conformation. This conformational preference is attributed to the enhancement of back-donation of the electron density towards π-accepting ligands. The correlation between the conformation of the RhS_2P_2N metallocycle and the electronic properties of the ligands coordinated *trans* to (^{Ph}L–*E*,*E*′)$^-$ (E = S, Se) is verified by a detailed computational study utilizing relativistic density functional theory. The boat conformation renders the two Rh–E bonds nonequivalent, which suggests a potential hemilabile behaviour of the (L–*E*,*E*′)$^-$ ligands. The latter is crucial for the catalytic activation of this type of complex. The interconnection between electronic properties and structural preferences presented herein can be used as a guide for the proper modification of the peripheral groups of the chalcogenidoimidodiphosphinato ligands to further enhance their hemilabile properties.

The catalytic activity against styrene hydroformylation of complexes **1**–**4** was explored and compared with the substantial catalytic activity of **6**, as well as the lack of activity of **5**.[50] Among **1**–**4**, complex **3** shows only poor catalytic activity, whereas the remaining complexes are essentially inactive. In fact, catalytic activity depends on the electronegativity of the chalcogenide donor atom (Se < S < O). This trend was elucidated with the aid of DFT-based computational methods using truncated model complexes. Activation of the complexes containing the softer chalcogenides S and Se towards catalytically active [Rh^I–H] species can proceed through the step-wise (i) H_2 side-on coordination, (ii) H_2 oxidative addition and (iii) hydride reductive elimination by means of an intramolecular acid–base reaction. However, the [Rh^{III}–$(H)_2$] species that are generated during the oxidative addition step are calculated as the most stable intermediates. Moreover, the subsequent hydride reductive elimination step by the (L–*E*,*E*)$^-$ ligand (E = S, Se) is both kinetically and thermodynamically not favoured, as can be deduced from the respective relaxed PES scan along the H–H bond-cleavage pathway (Figure 8). On the contrary, complex **6**, containing the harder oxygen atom in the Rh^I coordination sphere is activated through an alternative mechanism during which H_2 is directly heterolytically split. The oxygen atom acts as a base that polarizes the H–H bond and promotes its heterolytic cleavage. This gives rise to a catalytically active [Rh^I–H] species in which the oxygen atom of the ligand is protonated. This type of ligand-assisted activation by H_2 has been proposed for late-transition-metal complexes[86–93] as well as main-group compounds.[94]

Overall, this revisiting work on the mono- and dichalcogenidoimidodiphosphinato ligands aims to interpret the experimentally observed different catalytic properties of the respective Rh^I complexes against olefin hydroformylation. Future experimental work will benefit from these findings regarding the hemilabile and cooperative nature of this family of ligands to design more efficient catalytic systems.

Experimental Section

IR and NMR Spectroscopy: IR spectra were recorded in the range 4000–200 cm^{-1} on a Perkin–Elmer 883 IR spectrophotometer with samples as KBr discs. ^{1}H and ^{31}P spectra were recorded in a Varian Unity Plus 300 MHz instrument, operating at 299.95 and 121 MHz, respectively, using $CDCl_3$ as solvent. The ^{1}H and ^{31}P chemical shifts are relative to $SiMe_4$ and 85% H_3PO_4, respectively. Electrospray mass spectra were acquired on an MDX Sciex API Qstar Pulsar mass spectrometer (Toronto, Canada) using an electrospray ionization source.

X-ray Crystal Structure Determination: A brief summary of crystal data for complexes **1** and **3** is presented in the Supporting Information (Table S1). A crystal of **1** (yellow plate) was mounted in air. Diffraction data were measured at room temperature using a Syntex diffractometer equipped with a Rigaku rotating anode (graphite monochromator Cu-K_α radiation, λ = 1.5418 Å) by employing the $\theta/2\theta$ scanning method. Three standard reflections, monitored every 97 reflections, showed no decay in intensity during data collection. The data were corrected for Lorentz and polarization effects and a semiempirical absorption correction, based on the psi scans, was applied.[95] The structure was solved in the space group $P\bar{1}$ by direct methods with SHELXS[96] and was refined by full-matrix least-squares cycles based on F^2 with SHELXL-97.[96] All H atoms were placed in idealized positions and refined by a riding model (U_H = 1.30 U_C). All non-H atoms were modelled with anisotropic displacement parameters.

A crystal of **3** (yellow plate) was mounted on a glass fibre using perfluoropolyether oil and was cooled rapidly to 150 K in a stream of cold N_2 using an Oxford Cryosystems Cryostream unit. Diffraction data were measured using an Enraf–Nonius Kappa CCD diffractometer (graphite monochromator, Mo-K_α radiation, λ = 0.71073 Å). The structure was solved in the space group $P\bar{1}$ using

the direct methods program SIR-92,[97] which located all non-hydrogen atoms. Coordinates and anisotropic thermal parameters of all non-hydrogen atoms were refined. Hydrogen atoms were positioned geometrically after each cycle of refinement. A three-term Chebychev polynomial weighting scheme was applied.

CCDC-668479 (for **3**) and -668480 (for **1**) contain the supplementary crystallographic data for this paper. These data can be obtained free of charge from The Cambridge Crystallographic Data Centre via www.ccdc.cam.ac.uk/data_request/cif.

Computational Details: All calculations were performed with the ORCA computational package (version 2.9).[11] The BP86[98,99] functional was chosen for geometries, frequencies and electronic properties, respectively. The Ahlrichs polarized triple-ζ-quality basis sets TZVPP and TZVP[100] were used for the Rh center and the ligand atoms, respectively, in combination with the TZV/J Coulomb fitting basis for the resolution of identity[101,102] (RI in BP86 calculations). For geometry optimizations, a one-centre relativistic correction was applied by employing the implemented standard second-order Douglas–Kroll–Hess (DKH) procedure.[103–105] The structures were optimized in the gas phase at the RI-BP86/TZVPP/TZVP level together with the Grimme's dispersion correction.[106,107] Frequencies were calculated using a numerical differentiation of analytic gradients with an increment of 0.005 Bohr. Zero-point vibrational energies, thermal corrections and Gibbs free energies were obtained from the frequency calculations at the dispersion-corrected RI-BP86-D/TZVPP/TZVP level. Localized orbitals were computed according to the Pipek–Mezey population localization scheme[108] Calculations were performed on whole complexes starting from crystallographic coordinates, imposing both the boat and the twisted-boat conformation on the respective metallocycles and allowing all the geometric parameters to fully relax. In addition, truncated models were constructed in which the phenyl groups were replaced by methyl groups. The total electronic energy of the free reactants, that is, the initial rhodium complex and H_2, was always set as the zero point of reference for all the relaxed PES scans presented herein.

Synthesis: All synthetic manipulations were carried out under a pure-nitrogen atmosphere using standard Schlenk techniques. The glassware was dried in the oven at approximately 110 °C and baked out under vacuum prior to use. CH_3OH and CH_2Cl_2 were dried with CaH_2. THF and *n*-hexane were dried with Na wire/benzophenone. All solvents were distilled under N_2 and deoxygenated by three pump and purge cycles immediately prior to use. The protonated ligands (^{R}LH–*P*,*E*) and (^{R}LH–*E*,*E*′) and their corresponding potassium salts were prepared according to published procedures.[6,70,109,110] All other chemical reagents were purchased from Aldrich. PPh_3 was recrystallized from hot ethanol/water prior to use.

[Rh(^{Ph}L–*S*,*S*)(cod)] (1): A mixture of [{Rh(μ-Cl)(cod)}$_2$] (0.151 g, 0.30 mmol) and (^{Ph}L–*S*,*S*)K (0.293 g, 0.60 mmol) in THF (20 mL) was stirred for approximately 1 h at room temperature. The solvent was evaporated under vacuum and the solid residue was dissolved in CH_2Cl_2 (10 mL). The resulting solution was filtered through Celite to remove KCl. The filtrate was concentrated to 1–2 mL and layering with hexane (30 mL) afforded yellow crystals with 70% yield. $C_{32}H_{32}NP_2RhS_2$ (659.59): calcd. C 58.27, H 4.89, N 2.12, S 9.72; found C 58.54, H 4.71, N 2.62, S 9.86. ^{1}H NMR ($CDCl_3$): δ_H = 7.91 (m, 8 H, *m*-C_6H_5), 7.39 (m, 12 H, *o*,*p*-C_6H_5), 4.21 (s, 4 H, CH), 2.18 (m, 4 H, CH_2) 1.77 (m, 4 H, CH_2) ppm. ^{31}P{^{1}H} NMR ($CDCl_3$): δ_P = 38.8 (d, $^2J_{Rh,P}$ = 3.6 Hz) ppm. IR (KBr): $\tilde{\nu}$ = (CH) 3045–2823 (m); ν(PNP) 1167 (br); ν(PS) 575 (m) cm^{-1}. ES-MS: *m*/*z* = 660.1 [M + H]$^+$.

[Rh(^{Ph}L–*S*,*S*)(CO)$_2$] (2): Complex **1** (0.025g = 0.038 mmol) was dissolved in CH_2Cl_2 (10 mL). Carbon monoxide was then passed through the solution for 15 min. The mixture was concentrated under vacuum to 2–3 mL and layering with hexane (30 mL) afforded the yellow solid product with 87% yield. ^{1}H NMR ($CDCl_3$): δ_H = 7.91 (m, 8 H, aromatics), 7.42 (m, 12 H, aromatics) ppm. ^{31}P{^{1}H} NMR ($CDCl_3$, –60°): δ_P = 37.7 (d, $^2J_{Rh,P}$ = 3.6 Hz) ppm. IR (KBr): $\tilde{\nu}$ = (CO) 2066 (vs), 1997 (vs); ν(PNP) 1169 (br); ν(PS) 572 (m) cm^{-1}.

[Rh(^{Ph}L–*S*,*S*)(CO)(PPh$_3$)] (3): A mixture of complex **3** (0.020 g, 0.033 mmol) and PPh_3 (0.009 g = 0.034 mmol) in CH_2Cl_2 (10 mL) was stirred for approximately 2 h and then concentrated to 2–3 mL under vacuum. Layering with *n*-hexane (30 mL) afforded yellow crystals with 86% yield. $C_{43}H_{35}NOP_3RhS_2$ (841.70): calcd. C 61.36, H 4.19, N 1.66, S 7.62; found C 61.18, H 3.30, N 1.65, S 8.51. ^{1}H NMR ($CDCl_3$): δ_H = 7.93 (m, 8 H, *m*-C_6H_5), 7.43 (m, 12 H, *o*,*p*-C_6H_5), 7.50 (m, 15 H, PC_6H_5) ppm. ^{31}P{^{1}H} NMR ($CDCl_3$): δ_P = 40.5 (m, P_X, $^1J_{Rh,P_X}$ = 157 Hz, $^3J_{P_A,P_X}$ = 24 Hz); 38.3 (dd, P_B, $^2J_{Rh,P_B}$ = 4.1 Hz, $^3J_{P_B,P_X}$ = 8 Hz), 36.1 (dd, P_A, $^2J_{Rh,P_A}$ = 3.3 Hz, $^3J_{P_A,P_X}$ = 24 Hz) ppm, in which P_A is coordinated *trans* and P_B is coordinated *cis* to P_XPh_3. IR (KBr): $\tilde{\nu}$ = (CO) 1977 (vs); ν(PNP) 1161 (sh), 1151 (br); ν(PS) 563 (m) cm^{-1}.

[Rh(^{iPr}L–*S*,*S*)(cod)] (4): A mixture of [{Rh(μ-Cl)(cod)}$_2$] (0.050 g, 0.101 mmol) and (^{iPr}L–*S*,*S*)K (0.063 g, 0.202 mmol) in CH_2Cl_2 (10 mL) was stirred for approximately 2 h at room temperature. The solvent was evaporated under vacuum and the solid residue was dissolved in diethyl ether (10 mL). The resulting solution was filtered through Celite to remove KCl. Slow evaporation of the filtrate afforded yellow crystals with 55% yield. $C_{20}H_{40}NP_2RhS_2$ (523.52): calcd. C 45.88, H 7.70, N 2.68, S 12.25; found C 46.13, H 7.95, N 2.45, S 12.08. ^{1}H NMR ($CDCl_3$): δ_H = 4.16 (s, 4 H, CH), 2.37 (m, 4 H, CH_2), 2.07 (m, 2 H, CH-*i*Pr), 1.86 (m, 4 H, CH_2), 1.23 (m, 6 H, CH_3-*i*Pr) ppm. ^{31}P{^{1}H} NMR ($CDCl_3$): δ_P = 62.7 (br) ppm. IR (KBr): $\tilde{\nu}$ = (CH) 2918–2800 (m); ν(PNP) 1194 (br); ν(PS) 486 (m) cm^{-1}. ES-MS: *m*/*z* = 524.1 [M + H]$^+$.

Styrene Hydroformylation: In a typical experiment, styrene (2 mL, 17.5 mmol) and a solution of the corresponding rhodium complex in CH_2Cl_2 (3 mL, 0.012 mmol) were placed under argon in a stainless-steel autoclave with magnetic stirring, which was then sealed, pressurized with syngas (1:1 CO–H_2 mixture) to the appropriate pressure and brought to the desired temperature. After the required reaction time, the autoclave was cooled to room temperature, the pressure was carefully released and the solution was diluted with CH_2Cl_2, passed through Celite and catalytic conversions were determined by gas chromatography.

Supporting Information (see footnote on the first page of this article): Selected crystal data for complexes **1** and **3** (Table S1); comparison between the optimized geometry and the crystal structure of complex **3** (Table S2); Cartesian coordinates of all the optimized geometry structures (Tables S3–S12); buried volume values for different phosphane ligands (Table S13).

Acknowledgments

This research was financially supported by the Special Research Account of the National and Kapodistrian University of Athens (grant number 7575), by the European Social Fund (75% contribution), and by the National Resources (25% contribution) within the program EPEAEK II in the framework of the project "Pythagoras – Support of University Research Groups". The authors thank Dr. I. M. Mavridis for providing X-ray diffraction facilities at the

Laboratory of Structural and Supramolecular Chemistry, NCSR "Demokritos". P. K. is participating in the activities of Cost Action CM0802 (PhoSciNet) and thanks the Cost Office for funding, as well as the rest of the PhoSciNet members, especially Dr. I. D. Kostas, for helpful discussions. The reviewers of the manuscript are accredited for their constructive comments.

[1] T. Q. Ly, J. D. Woollins, *Coord. Chem. Rev.* **1998**, *176*, 451.
[2] J. D. Woollins, *J. Chem. Soc., Dalton Trans.* **1996**, 2893.
[3] C. Silvestru, J. E. Drake, *Coord. Chem. Rev.* **2001**, *223*, 117.
[4] I. Haiduc, *J. Organomet. Chem.* **2001**, *623*, 29.
[5] I. Haiduc, in: *Comprehensive Coordination Chemistry II* (Eds.: J. A. McCleverty, T. J. Meyer), Pergamon, Oxford, UK, **2003**, p. 323.
[6] P. Bhattacharyya, J. Novosad, J. Phillips, A. M. Z. Slawin, D. J. Williams, J. D. Woollins, *J. Chem. Soc., Dalton Trans.* **1995**, 1607.
[7] R. Rosler, C. Silvestru, G. Espinosa-Perez, I. Haiduc, R. Cea-Olivares, *Inorg. Chim. Acta* **1996**, *241*, 47.
[8] E. Simon-Manso, M. Valderrama, D. Boys, *Inorg. Chem.* **2001**, *40*, 3647.
[9] N. Levesanos, S. D. Robertson, D. Maganas, C. P. Raptopoulou, A. Terzis, P. Kyritsis, T. Chivers, *Inorg. Chem.* **2008**, *47*, 2949.
[10] E. Ferentinos, D. Maganas, C. P. Raptopoulou, A. Terzis, V. Psycharis, N. Robertson, P. Kyritsis, *Dalton Trans.* **2011**, *40*, 169.
[11] D. Maganas, J. Krzystek, E. Ferentinos, A. M. Whyte, N. Robertson, V. Psycharis, A. Terzis, F. Neese, P. Kyritsis, *Inorg. Chem.* **2012**, *51*, 7218.
[12] D. Maganas, S. S. Staniland, A. Grigoropoulos, F. White, S. Parsons, N. Robertson, P. Kyritsis, G. Pneumatikakis, *Dalton Trans.* **2006**, 2301.
[13] G. Mathies, S. D. Chatziefthimiou, D. Maganas, Y. Sanakis, S. Sottini, P. Kyritsis, E. J. J. Groenen, *J. Magn. Reson.* **2012**, *224*, 94.
[14] S. Sottini, G. Mathies, P. Gast, D. Maganas, P. Kyritsis, E. J. J. Groenen, *Phys. Chem. Chem. Phys.* **2009**, *11*, 6727.
[15] D. Maganas, S. Milikisyants, J. M. A. Rijnbeek, S. Sottini, N. Levesanos, P. Kyritsis, E. J. J. Groenen, *Inorg. Chem.* **2010**, *49*, 595.
[16] D. Maganas, S. Sottini, P. Kyritsis, E. J. J. Groenen, F. Neese, *Inorg. Chem.* **2011**, *50*, 8741.
[17] D. Maganas, A. Grigoropoulos, S. S. Staniland, S. D. Chatziefthimiou, A. Harrison, N. Robertson, P. Kyritsis, F. Neese, *Inorg. Chem.* **2010**, *49*, 5079.
[18] Z. Dauter, K. S. Wilson, L. C. Sieker, J. M. Moulis, J. Meyer, *Proc. Natl. Acad. Sci. USA* **1996**, *93*, 8836.
[19] M. Maher, M. Cross, M. C. J. Wilce, J. M. Guss, A. G. Wedd, *Acta Crystallogr., Sect. D* **2004**, *60*, 298.
[20] G. G. Briand, T. Chivers, M. Parvez, *Angew. Chem.* **2002**, *114*, 3618; *Angew. Chem. Int. Ed.* **2002**, *41*, 3468.
[21] T. Chivers, J. S. Ritch, S. D. Robertson, J. Konu, H. M. Tuononen, *Acc. Chem. Res.* **2010**, *43*, 1053.
[22] J. S. Ritch, T. Chivers, M. Afzaal, P. O'Brien, *Chem. Soc. Rev.* **2007**, *36*, 1622.
[23] C. Q. Nguyen, M. Afzaal, M. A. Malik, M. Helliwell, J. Raftery, P. O'Brien, *J. Organomet. Chem.* **2007**, *692*, 2669.
[24] M. Afzaal, D. Crouch, M. A. Malik, M. Motevalli, P. O'Brien, J. H. Park, J. D. Woollins, *Eur. J. Inorg. Chem.* **2004**, 171.
[25] M. Afzaal, K. Ellwood, N. L. Pickett, P. O'Brien, J. Raftery, J. Waters, *J. Mater. Chem.* **2004**, *14*, 1310.
[26] D. Oyetunde, M. Afzaal, M. A. Vincent, I. H. Hillier, P. O'Brien, *Inorg. Chem.* **2011**, *50*, 2052.
[27] J. S. Ritch, T. Chivers, K. Ahmad, M. Afzaal, P. O'Brien, *Inorg. Chem.* **2010**, *49*, 1198.
[28] A. Panneerselvam, M. A. Malik, M. Afzaal, P. O'Brien, M. Helliwell, *J. Am. Chem. Soc.* **2008**, *130*, 2420.
[29] G. L. Abbati, M. C. Aragoni, M. Arca, M. B. Carrea, F. A. Devillanova, A. Garau, F. Isaia, V. Lippolis, M. Marcelli, C. Silvestru, G. Verani, *Eur. J. Inorg. Chem.* **2005**, 589.
[30] G. L. Abbati, M. C. Aragoni, M. Arca, F. A. Devillanova, A. C. Fabretti, A. Garau, F. Isaia, V. Lippolis, G. Verani, *Dalton Trans.* **2003**, 1515.
[31] M. C. Aragoni, M. Arca, M. B. Carrea, F. Demartin, F. A. Devillanova, A. Garau, F. Isaia, V. Lippolis, G. Verani, *Eur. J. Inorg. Chem.* **2004**, 4660.
[32] B. A. Demko, R. E. Wasylishen, *Dalton Trans.* **2008**, 481.
[33] B. A. Demko, R. E. Wasylishen, *Inorg. Chem.* **2008**, *47*, 2786.
[34] S. W. Magennis, S. Parsons, Z. Pikramenou, *Chem. Eur. J.* **2002**, *8*, 5761.
[35] M. A. Katkova, M. E. Burin, A. A. Logunov, V. A. Ilichev, A. N. Konev, G. K. Fukin, M. N. Bochkarev, *Synth. Met.* **2009**, *159*, 1398.
[36] A. P. Bassett, D. R. Van, P. Nockemann, P. B. Glover, B. M. Kariuki, H. K. Van, M. L. Van, Z. Pikramenou, *Inorg. Chem.* **2005**, *44*, 6140.
[37] P. B. Glover, A. P. Bassett, P. Nockemann, B. M. Kariuki, D. R. Van, Z. Pikramenou, *Chem. Eur. J.* **2007**, *13*, 6308.
[38] G. Mancino, A. J. Ferguson, A. Beeby, N. J. Long, T. S. Jones, *J. Am. Chem. Soc.* **2005**, *127*, 524.
[39] A. J. Gaunt, B. L. Scott, M. P. Neu, *Angew. Chem.* **2006**, *118*, 1668; *Angew. Chem. Int. Ed.* **2006**, *45*, 1638.
[40] A. J. Gaunt, B. L. Scott, M. P. Neu, *Chem. Commun.* **2005**, 3215.
[41] A. J. Gaunt, S. D. Reilly, A. E. Enriquez, B. L. Scott, J. A. Ibers, P. Sekar, K. I. M. Ingram, N. Kaltsoyannis, M. P. Neu, *Inorg. Chem.* **2007**, *46*, 29.
[42] K. I. M. Ingram, M. J. Tassell, A. J. Gaunt, N. Kaltsoyannis, *Inorg. Chem.* **2008**, *47*, 7824.
[43] W.-H. Leung, K.-K. Lau, Q.-f. Zhang, W.-T. Wong, B. Tang, *Organometallics* **2000**, *19*, 2084.
[44] X.-Y. Yi, G. K. Y. Ng, I. D. Williams, W.-H. Leung, *Inorg. Chim. Acta* **2006**, *359*, 3581.
[45] W.-M. Cheung, H.-Y. Ng, I. D. Williams, W.-H. Leung, *Inorg. Chem.* **2008**, *47*, 4383.
[46] G.-C. Wang, H. H. Y. Sung, I. D. Williams, W.-H. Leung, *Inorg. Chem.* **2012**, *51*, 3640.
[47] D. K. Dutta, B. Deb, *Coord. Chem. Rev.* **2011**, *255*, 1686.
[48] F. Bonati, G. Wilkinson, *J. Chem. Soc.* **1964**, 3156.
[49] A. M. Trzeciak, B. Borak, Z. Ciunik, J. J. Ziółkowski, M. da Silva, A. J. L. Pombeiro, *Eur. J. Inorg. Chem.* **2004**, 1411.
[50] K. A. Chatziapostolou, K. A. Vallianatou, A. Grigoropoulos, C. P. Raptopoulou, A. Terzis, I. D. Kostas, P. Kyritsis, G. Pneumatikakis, *J. Organomet. Chem.* **2007**, *692*, 4129.
[51] E. Lindner, Q. Wang, H. A. Mayer, A. Bader, H. Kuehbauch, P. Wegner, *Organometallics* **1993**, *12*, 3291.
[52] E. Lindner, Q. Wang, H. A. Mayer, R. Fawzi, M. Steimann, *Organometallics* **1993**, *12*, 1865.
[53] A. Bader, E. Lindner, *Coord. Chem. Rev.* **1991**, *108*, 27.
[54] P. Braunstein, F. Naud, *Angew. Chem.* **2001**, *113*, 702; *Angew. Chem. Int. Ed.* **2001**, *40*, 680.
[55] T. Matsubara, N. Koga, Y. Ding, D. G. Musaev, K. Morokuma, *Organometallics* **1997**, *16*, 1065.
[56] D. Gleich, J. Hutter, *Chem. Eur. J.* **2004**, *10*, 2435.
[57] X. Luo, D. Tang, M. Li, *Int. J. Quantum Chem.* **2006**, *106*, 1844.
[58] M. Sparta, K. J. Børve, V. R. Jensen, *J. Am. Chem. Soc.* **2007**, *129*, 8487.
[59] C. J. Cramer, D. G. Truhlar, *Phys. Chem. Chem. Phys.* **2009**, *11*, 10757.
[60] A. Anoop, W. Thiel, F. Neese, *J. Chem. Theory Comput.* **2010**, *6*, 3137.
[61] J. G. Leipoldt, G. J. Lamprecht, E. C. Steynberg, *J. Organomet. Chem.* **1990**, *397*, 239.
[62] A. M. Trzeciak, T. Glowiak, R. Grzybek, J. J. Ziółkowski, *J. Chem. Soc., Dalton Trans.* **1997**, 1831.

[63] P. B. Hitchcock, J. F. Nixon, I. Silaghi-Dumitrescu, I. Haiduc, *Inorg. Chim. Acta* **1985**, *96*, 77.
[64] A. M. Z. Slawin, J. Ward, D. J. Williams, J. D. Woollins, *J. Chem. Soc., Chem. Commun.* **1994**, 421.
[65] L. Nyulaszi, T. Veszpremi, J. Reffy, *J. Phys. Chem.* **1995**, *99*, 10142.
[66] L. Nyulaszi, T. Veszpremi, *J. Phys. Chem.* **1996**, *100*, 6456.
[67] C. W. Tate, P. B. Hitchcock, G. A. Lawless, Z. Benko, L. Nyulaszi, J. F. Nixon, *C. R. Chim.* **2010**, *13*, 1063.
[68] L. M. Gilby, B. Piggott, *Polyhedron* **1999**, *18*, 1077.
[69] W.-M. Cheung, C.-Y. Lai, Q.-F. Zhang, W.-Y. Wong, I. D. Williams, W.-H. Leung, *Inorg. Chim. Acta* **2006**, *359*, 2712.
[70] D. Cupertino, R. Keyte, A. M. Z. Slawin, D. J. Williams, J. D. Woollins, *Inorg. Chem.* **1996**, *35*, 2695.
[71] D. Cupertino, R. Keyte, A. M. Z. Slawin, J. D. Woollins, D. J. Williams, *Polyhedron* **1996**, *15*, 4441.
[72] T. G. Appleton, H. C. Clark, L. E. Manzer, *Coord. Chem. Rev.* **1973**, *10*, 335.
[73] J. G. Leipoldt, S. S. Basson, L. D. C. Box, T. I. A. Gerber, *Inorg. Chim. Acta* **1978**, *26*, L35.
[74] P. Braunstein, Y. Chauvin, J. Nahring, A. DeCian, J. Fischer, A. Tiripicchio, F. Ugozzoli, *Organometallics* **1996**, *15*, 5551.
[75] M. Lamac, I. Cisarova, P. Stepnicka, *J. Organomet. Chem.* **2005**, *690*, 4285.
[76] P. Stepnicka, I. Cisarova, *J. Chem. Soc., Dalton Trans.* **1998**, 2807.
[77] A. M. Trzeciak, J. J. Ziółkowski, T. Lis, R. Choukroun, *J. Organomet. Chem.* **1999**, *575*, 87.
[78] C. A. Tolman, *Chem. Rev.* **1977**, *77*, 313.
[79] P. W. N. M. van Leeuwen, C. Claver, *Rhodium Catalyzed Hydroformylation*, Kluwer, Dordrecht, The Netherlands, **2002**.
[80] R. H. Crabtree, *Angew. Chem.* **1993**, *105*, 828; *Angew. Chem. Int. Ed. Engl.* **1993**, *32*, 789.
[81] G. J. Kubas, *Proc. Natl. Acad. Sci. USA* **2007**, *104*, 6901.
[82] S. Aldridge, A. J. Downs, *Chem. Rev.* **2001**, *101*, 3305.
[83] G. J. Kubas, *Chem. Rev.* **2007**, *107*, 4152.
[84] G. J. Kubas, *J. Organomet. Chem.* **2009**, *694*, 2648.
[85] A. Poater, B. Cosenza, A. Correa, S. Giudice, F. Ragone, V. Scarano, L. Cavallo, *Eur. J. Inorg. Chem.* **2009**, 1759.
[86] J. Andrieu, J. M. Camus, P. Richard, R. Poli, L. Gonsalvi, F. Vizza, M. Peruzzini, *Eur. J. Inorg. Chem.* **2006**, 51.
[87] J. Meeuwissen, A. J. Sandee, B. de Bruin, M. A. Siegler, A. L. Spek, J. N. H. Reek, *Organometallics* **2010**, *29*, 2413.
[88] A. Ienco, M. J. Calhorda, J. Reinhold, F. Reineri, C. Bianchini, M. Peruzzini, F. Vizza, C. Mealli, *J. Am. Chem. Soc.* **2004**, *126*, 11954.
[89] P. Maire, T. Böttner, F. Breher, P. Le Floch, H. Grützmacher, *Angew. Chem.* **2005**, *117*, 6477; *Angew. Chem. Int. Ed.* **2005**, *44*, 6318.
[90] J. Andrieu, J. M. Camus, C. Balan, R. Poli, *Eur. J. Inorg. Chem.* **2006**, 62.
[91] A. Rossin, L. Gonsalvi, A. D. Phillips, O. Maresca, A. Lledos, M. Peruzzini, *Organometallics* **2007**, *26*, 3289.
[92] A. M. Trzeciak, P. Stepnicka, E. Mieczynska, J. J. Ziółkowski, *J. Organomet. Chem.* **2005**, *690*, 3260.
[93] T. He, N. P. Tsvetkov, J. G. Andino, X. Gao, B. C. Fullmer, K. G. Caulton, *J. Am. Chem. Soc.* **2009**, *132*, 910.
[94] L. Könczöl, E. Makkos, D. Bourissou, D. Szieberth, *Angew. Chem. Int. Ed.* **2012**, *51*, 9521.
[95] A. C. T. North, D. C. Phillips, F. S. Mathews, *Acta Crystallogr., Sect. A* **1968**, *24*, 351.
[96] G. Sheldrick, *Acta Crystallogr., Sect. A* **2008**, *64*, 112.
[97] A. Altomare, G. Cascarano, C. Giacovazzo, A. Guagliardi, M. C. Burla, G. Polidori, M. Camalli, *J. Appl. Crystallogr.* **1994**, *27*, 435.
[98] A. D. Becke, *Phys. Rev. A* **1988**, *38*, 3098.
[99] J. P. Perdew, *Phys. Rev. B* **1986**, *33*, 8822.
[100] A. Schäfer, C. Huber, R. Ahlrichs, *J. Chem. Phys.* **1994**, *100*, 5829.
[101] M. Feyereisen, G. Fitzgerald, A. Komornicki, *Chem. Phys. Lett.* **1993**, *208*, 359.
[102] R. A. Kendall, H. A. Früchtl, *Theor. Chem. Acc.* **1997**, *97*, 158.
[103] B. A. Hess, *Phys. Rev. A* **1985**, *32*, 756.
[104] B. A. Hess, *Phys. Rev. A* **1986**, *333*, 3742.
[105] G. Jansen, B. A. Hess, *Phys. Rev. A* **1989**, *39*, 6016.
[106] S. Grimme, J. Antony, S. Ehrlich, H. Krieg, *J. Chem. Phys.* **2010**, *132*, 154104.
[107] S. Grimme, S. Ehrlich, L. Goerigk, *J. Comput. Chem.* **2011**, *32*, 1456.
[108] J. Pipek, P. G. Mezey, *J. Chem. Phys.* **1989**, *90*, 4916.
[109] F. T. Wang, J. Najdzionek, K. L. Leneker, H. Wasserman, D. M. Braitsch, *Synth. React. Inorg. Met. Org. Chem.* **1978**, *8*, 119.
[110] D. J. Birdsall, A. M. Z. Slawin, J. D. Woollins, *Polyhedron* **2001**, *20*, 125.

Received: August 10, 2012
Published Online: December 19, 2012

